Fatigue crack growth in a laser shock peened residual stress field

Pavan, M., Furfari, D., Ahmad, B., Gharghouri, M. A. & Fitzpatrick, M. E.

Fatigue Crack Growth in a Laser Shock Peened Residual Stress Field

M.Pavan[1], D.Furfari[2], B.Ahmad[1], M.A.Gharghouri[3], M.E.Fitzpatrick[1]

[1]*Coventry University, Priory Street, Coventry, United Kingdom, CV1 5FB*

[2]*Airbus Operations GmbH, Kreetslag 10, Hamburg, Germany, 21129*

[3]*Canadian Nuclear Laboratories, Chalk River, Ontario, Canada, K0J 1J0*

marco.pavan@coventry.ac.uk*, +44 (0) 24 7765 7688*

Abstract

Laser Shock Peening is a surface treatment technique used in the aerospace sector to increase fatigue life, as well as resistance to fretting fatigue and stress corrosion cracking. In this study, laser shock peening was applied to a 6-mm-thick middle-crack tension specimen made of aluminium 2524-T351. Residual stress was measured with neutron diffraction and the contour method, along the predicted crack path prior to fatigue testing. Fatigue crack growth test results showed that fatigue life improved by a factor of 4 compared to an untreated component, owing to a significant crack growth rate reduction inside the laser peened area. A linear-elastic finite-element crack growth prediction model was also developed, obtaining predicted results in excellent agreement with the experimental data.

1 Introduction

The use of laser shock peening has become increasingly popular owing to the decreasing cost of laser systems. The process has been shown to be more effective and controllable than similar techniques such as shot peening and deep rolling, especially in terms of residual stress introduced, providing furthermore a better surface roughness. A complete review of laser shock peening is provided in [1], while the fatigue life performance improvements achieved using this surface treatment for different metals are reported in [2–5]. In the laser shock peening process, a high energy laser pulse (1-100+ J) is fired at a metal target surface, usually covered with an ablative layer, also called a sacrificial layer. As the pulse reaches the target surface, because of the high energy involved (several GW/cm^2), the ablative layer vaporizes, creating a high-pressure plasma. The interaction of the high-pressure plasma with the metal surface generates a pressure pulse of several GPa. In order to maximize the energy transferred in the process, the

target surface is usually covered by a thin layer of flowing water, which confines the plasma between it and the metal surface. The pressure pulse produced propagates as a shockwave within the metal, locally overcoming the Hugoniot Elastic Limit and causing plastic deformation. As a result, a compressive residual stress is generated to a depth that depends on the process parameters but which can be several millimetres.

In the aeronautical sector today, laser shock peening is applied to specific critical engine components subjected to high loads, foreign object damage, and fretting fatigue, mainly to prevent or retard crack initiation and the early stages of crack propagation [1], [6]. Its application to airframe components, characterised by potentially longer cracks, has not yet been thoroughly investigated.

The effect of residual stress on fatigue life and fatigue crack propagation is of great importance in any engineering application and has been therefore widely studied since the development of Linear-Elastic Fracture Mechanics (LEFM). This approach allows the stress state near the crack tip to be described using linear equations, simplifying the effort to understand and predict crack propagation. Several techniques based on LEFM have been developed to deal with residual stress at the crack tip, such as the superposition and the modified superposition methods [7]. According to the superposition principle, the stress state due to two or more loads acting together is equal to the sum of each load acting separately, provided that the material behaviour is linear-elastic [8]. In a cyclically-loaded residual-stress-bearing body, the stresses due to applied mechanical loads are therefore linearly superimposed on the residual stresses. The superposition technique involves the calculation of two separate stress intensity factors, one associated with the applied load, K_L, and one associated with the residual stress, K_{Res} [7]. These two values are then summed to obtain the total stress intensity factor at the crack tip:

$$K_{max,TOT} = K_{max,L} + K_{Res} \quad (1)$$

$$K_{min,TOT} = K_{min,L} + K_{Res} \quad (2)$$

where $K_{max,L}$ and $K_{min,L}$ are the stress intensity factors at the maximum and minimum applied loads, respectively. The total stress intensity factor range is calculated as follows:

$$\Delta K_{TOT} = K_{max,TOT} - K_{min,TOT} = K_{max,L} + K_{Res} - K_{min,L} - K_{Res} = K_{max,L} - K_{min,L} \qquad (3)$$

Eq. (3) shows that the stress intensity factor range does not depend on the residual stress, since the K_{Res} contribution cancels out. However, the total stress ratio, R_{TOT}, does depend on the residual stress:

$$R_{TOT} = \frac{K_{min,TOT}}{K_{max,TOT}} = \frac{K_{min,L} + K_{Res}}{K_{max,L} + K_{Res}} \qquad (4)$$

and is therefore representative of the true conditions at the crack tip.

The effect of crack face contact, not considered in the superposition method, can be included in the stress intensity factor calculation using a modified superposition approach, in which $K_{min,TOT}$ is set to 0 in Eq. (2) whenever its value becomes negative, simulating crack closure. The total stress intensity factor range in this formulation becomes:

$$\Delta K_{TOT} = K_{max,TOT} - K_{min,TOT} \ \ \text{if} \ \ K_{min,TOT} > 0$$
$$\Delta K_{TOT} = K_{max,TOT} \ \ \text{if} \ \ K_{min,TOT} \leq 0 \qquad (5)$$

The total stress ratio is then:

$$R_{TOT} = \frac{K_{min,TOT}}{K_{max,TOT}} \ \text{if} \ \ K_{min,TOT} > 0$$
$$R_{TOT} = 0 \ \text{if} \ \ K_{min,TOT} \leq 0 \qquad (6)$$

Superposition-based techniques are commonly used owing to their simplicity, but they have been criticised as being incapable of accounting for the redistribution and relaxation of residual stress that accompanies crack propagation [9–12]. Even though ([13]) the redistribution and relaxation of stress associated with the presence of a crack does not invalidate the superposition principle, the use of FE models to calculate the residual stress intensity factor K_{Res} is often favoured since they naturally include these effects during crack growth.

An alternative approach to superposition-based techniques, referred to as Plasticity-Induced Crack Closure (PICC), was introduced in 1970 by Elber [14], who noticed that cracks in fatigue specimens are fully open only for a part of the loading cycle, even when the loading cycle is fully tensile. Elber argued that the closure phenomenon is an effect of the plastic deformation developed in the wake of the propagating crack, resulting in a compressive residual stress field which in turn causes the crack to close before the minimum load is reached, at a value of K_{op} instead of K_{min} ($K_{op} > K_{min}$), reducing the stress intensity factor range from ΔK to ΔK_{eff} according to the following equation:

$$\Delta K_{eff} = K_{max,TOT} - K_{op} \qquad (7)$$

where K_{op} represents the stress intensity factor at which the crack starts to open. Below this threshold, the crack faces are closed, therefore the part of the cycle for which the stress intensity factor is lower than K_{op} does not contribute to fatigue crack growth. The PICC approach requires the calculation of the opening stress intensity factor K_{op}, which is generally achieved through elastic-plastic finite element analysis or by using simpler analytical models such as Newman's [15,16].

Both superposition-based and crack-closure-based techniques have been successfully applied in the literature to predict crack growth rates in the presence of residual stress fields. A completely linear-elastic approach was used by Parker [13], who achieved good agreement with experimental data using the modified superposition method for different geometries and loading conditions; and by Hill and Kim [17], who compared superposition, modified superposition, superposition contact and a newly-developed superposition contact method. The authors considered a standard Compact-Tension (CT) specimen treated by laser shock peening over a square area surrounding the initial notch, calculating stress intensity factors and crack opening using weight functions. The different methods yielded very similar predictions for crack propagation within the laser peened area, where the effect of the compressive residual stress was predominant. However, the newly-developed superposition contact method gave better agreement with the experimental results for propagation outside of the peened areas, where the crack surfaces were only partially closed during the loading cycle.

A comparison between linear elastic and elastic-plastic finite element modelling applied to LEFM, with and without crack closure, was carried out by Garcia et al.in [18]. The authors studied the fatigue crack growth behaviour on a rectangular specimen made of AA7050-T7451 with residual stress introduced by four point bending, testing both positive and negative stress ratios. The crack closure behaviour was simulated with a rigid surface which did not allow a negative displacement of the crack faces, i.e. the faces could not inter-penetrate. Results highlighted how for a positive stress ratio the models with closure better approximated the test outcome in the compressive areas. The finite element elastic-plastic model provided crack growth rate results closer to the experimental data but constantly underestimated, resulting in a non-conservative fatigue-life estimation. For the negative stress ratio, the linear elastic approach without crack closure presented the best results.

A recent study by Kashev et al. [19], investigated the effect of laser shock peening on the microstructure and fatigue crack propagation behaviour of thin AA2024 CT specimens. The authors correlated the effect of the residual stress originated by the treatment, with the Crack Opening Displacement (COD) at different crack lengths. Results showed how compared to the baseline material, COD was increased or decreased depending whether the residual stress field encountered was tensile or compressive. Compressive residual stress caused the crack to open less, generating a beneficial crack closure effect.

In the current work, several techniques for predicting crack propagation are compared: superposition, modified-superposition and plasticity-induced crack closure based on Newman's analytical equations (henceforth referred to as the Newman method) [15][16].

2   Experimental Methods

The five specimens used in this study were supplied by Airbus Operations GmbH, Germany. They were made of a 2524-T351 clad aluminium alloy, commonly used for aircraft structural components such as wing lower covers. Each specimen was extracted from a rolled aluminium panel, such that the

longitudinal (stress) axis was parallel to the rolling direction. Typical mechanical properties for this aluminium alloy are reported in Table 1**Error! Reference source not found.**.

Table 1 – AA2524-T351 minimum tensile properties [20]

Orientation	Tensile Strength [MPa]	Yield Strength at 0.2% Offset [MPa]	Elongation at failure [%]
L-T	427	276	15

Each specimen was 200 mm wide, 400 mm long and 6 mm thick, as shown in Figure 1. Only three of the five specimens were laser shock peened, using the processing parameters described in the next section.
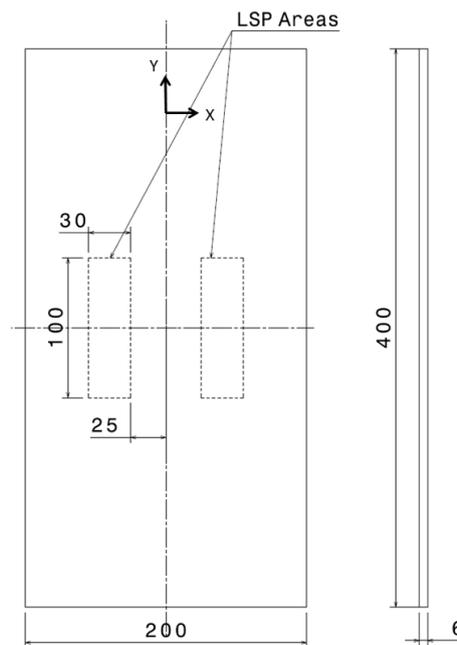

Figure 1 – Specimen dimensions in mm

2.1   Laser Shock Peening

The Laser Shock Peening (LSP) treatment was carried out by Metal Improvement Company, Earby, UK, using the parameters listed in Table 2**Error! Reference source not found.**.

Table 2 – Laser Shock Peening parameters

LSP	Power Density [GW/cm²]	Energy [J]	Spot Size [mm²]	Pulse Duration [ns]	Spot Offset	Spot Overlap	Layers
3-18-4	3	16	5.5 × 5.5	18	50%	5%	4

Each layer of treatment was applied sequentially on both sides, to generate a uniform compression through the thickness and limit the amount of geometric distortion. The full list of specimens tested is presented in Table 3**Error! Reference source not found.**.

Table 3 – Specimen designation, laser peening and loading conditions (AM=As Manufactured, LSP= Laser Shock Peened); BL signifies the baseline samples that were tested without peening

Designation	Condition	R_L	σ_{max} [MPa]
BL-1	AM	0.1	113
BL-2	AM	0.1	113
LSP-1	LSP	0.1	113
LSP-2	LSP	0.1	113
LSP-3	LSP		

2.2   Residual Stress Measurements

The residual stress along the predicted crack path was determined with neutron diffraction [2] and with the contour method [21] on the specimen LSP-3. Neutron diffraction measurements were carried out using the L3 diffractometer of the Canadian Neutron Beam Centre (CNBC) located in the NRU reactor of Canadian Nuclear Laboratories. The aluminium 311 reflection was used for the lattice strain measurements to obtain neutrons with a nominal wavelength of 1.727 Å, giving a scattering angle close to 90°. The x-, y-, and z- components of lattice strain were measured at 23 depths at three locations (Points 1-3) using a step size of 0.250 mm as shown in Figure 2. In addition to these depth profiles, thickness-averaged measurements of lattice strain were obtained along Line 1 (Figure 2) by oscillating the gauge volume continuously over the whole specimen thickness (6 mm) during each measurement.
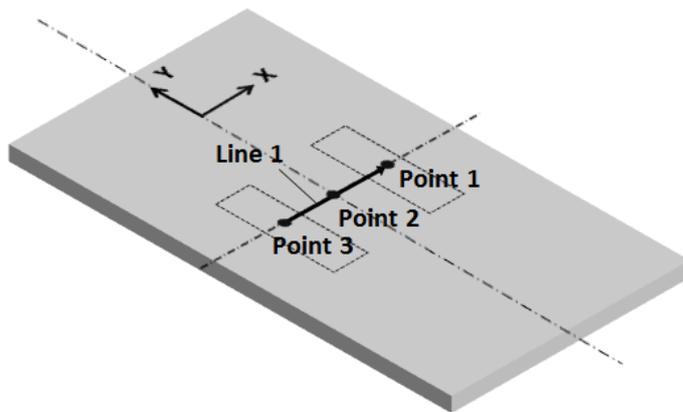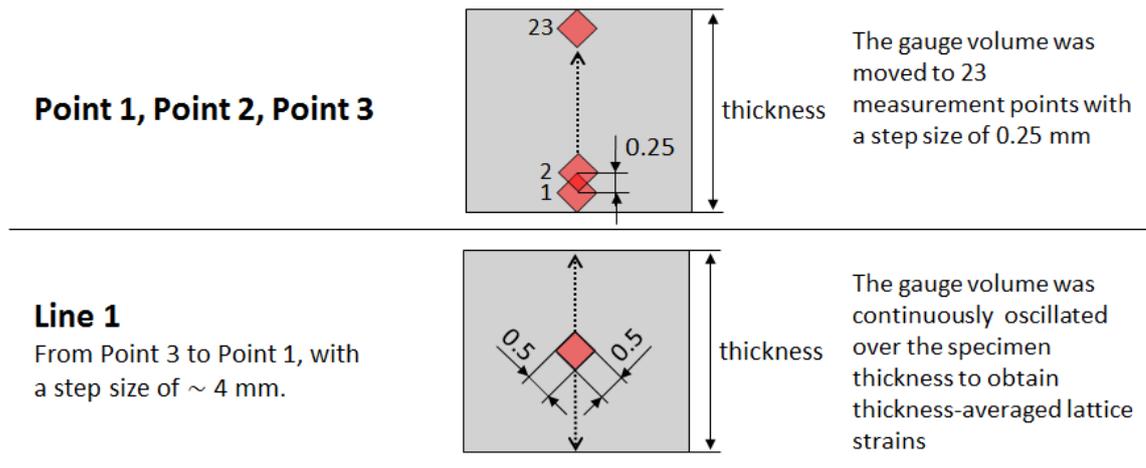
Point 1, Point 2, Point 3

23

thickness

0.25

2
1

The gauge volume was moved to 23 measurement points with a step size of 0.25 mm

Line 1
From Point 3 to Point 1, with a step size of ~ 4 mm.

0.5   0.5

thickness

The gauge volume was continuously oscillated over the specimen thickness to obtain thickness-averaged lattice strains

Line 1
Point 1
Point 2
Point 3

Figure 2 – Neutron Diffraction measurement point locations, dimensions in mm, not to scale

The contour method measurements were carried out at Coventry University on the plane shown in Figure 3**Error! Reference source not found.**. The specimen was cut in two halves by EDM cutting and the surface displacements originated from the stress relief were measured with a Zeiss Contra G2 Coordinate Measuring Machine. A point spacing of 0.2 mm was used in both directions on the cut surface, with a spherical probe of 3 mm diameter. The major benefit of the contour method is the production of a complete 2D map of residual stress over the cut surface. The drawback, however, is that only the component of residual stress normal to the cutting plane (Y direction in Figure 3**Error! Reference source not found.**) is obtained. The contour method is normally less accurate for the near surface results due to the errors arising from the wire EDM cutting and data smoothing. In this study, an effort was made to keep the power settings to a minimum value obtaining therefore a good surface finish, which in turn

decreased the EDM wire entry and exit artefacts improving the results. Due to the destructive nature of the method, the test was carried out after the neutron diffraction measurements on the same specimen.
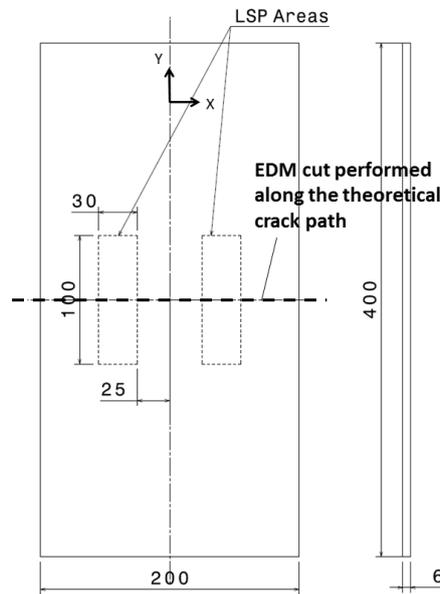

Figure 3 – Contour Method measurement plane

2.3 Fatigue Crack Growth Tests

A central notch was created by Electro-Discharge Machining (EDM) in both the laser peened and unpeened specimens to prepare them for fatigue crack growth testing, except for LSP-3 which was used only for residual stress measurements. The laser shock peening treatment was carried out prior to notch creation. All tests were carried out in laboratory air at ambient temperature (20°C) according to ASTM standard E647 [22]. The fatigue loading conditions were the following: σ_{max} = 113 MPa, R_L = 0.1, frequency = 10Hz, with an initial crack length including pre-cracking of 4 mm.

3 Numerical Modelling

The numerical modelling strategy consisted of three different steps as shown in Figure 4. In the first step, the residual stress is introduced into the specimen based on the neutron diffraction and contour method

results presented in section 2. In the second step, fatigue crack growth is simulated by advancing the crack and extracting the forces and displacements at the crack front from the model. In the final step, the extracted force and displacement information is used to calculate the stress intensity factors and the fatigue life according to the crack growth prediction models.
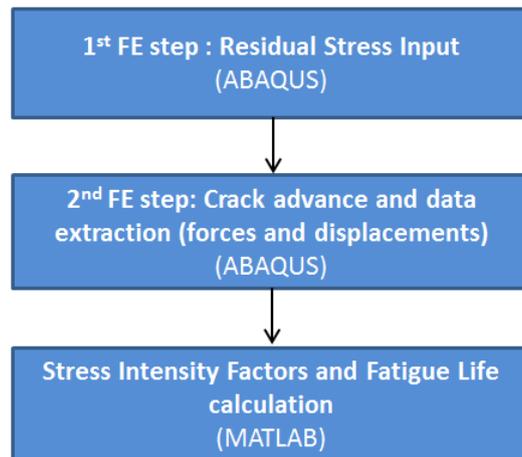

Figure 4 – Numerical modelling steps

The first and second steps were performed using the Finite Element (FE) software ABAQUS 6.14-1 [23], while the third step was performed using MATLAB 2013b [24]. A 3D rather than a 2D Finite Element model was preferred because 1) the specimen thickness (6 mm) is sufficient to develop a 3D state of stress, and 2) it allowed better control over the residual stress distribution introduced during the first step. To reduce the number of elements and the computation time, only a quarter of the overall specimen was simulated. Full integration eight-node linear brick elements were used (C3D8), with a linear elastic material behaviour based on the following parameters: Young's modulus $E = 73$ GPa, Poisson's ratio $v = 0.33$. A mesh sensitivity analysis was carried out, resulting in the mesh presented in Figure 5.
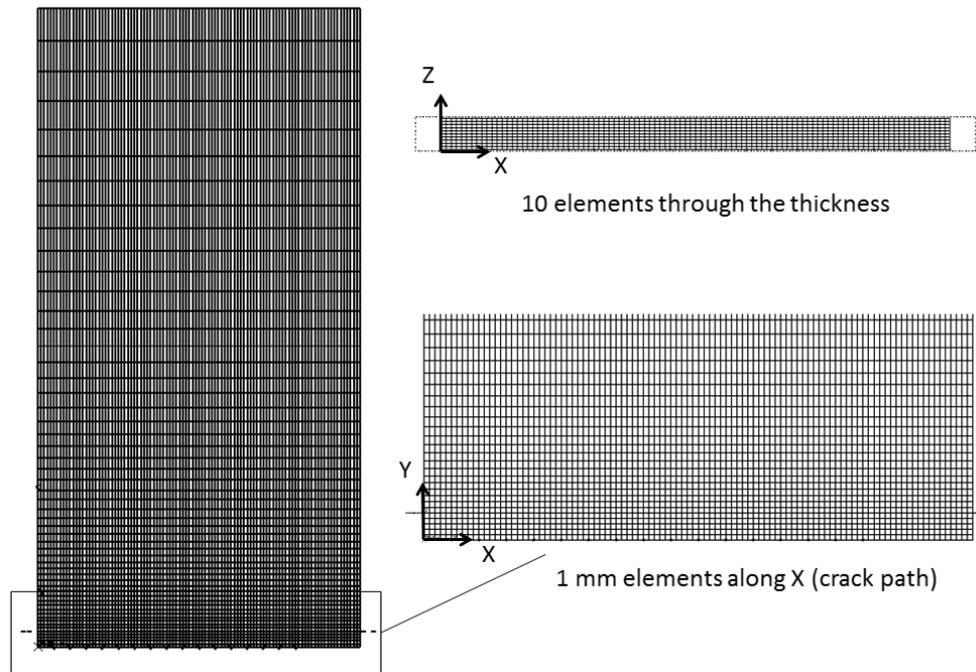
Figure 5 – Finite Element Mesh used to model a quarter of the M(T) specimen

3.1 Residual Stress Input

The residual stress was introduced into the FE model through the Abaqus user subroutine SIGINI, a FORTRAN program which initialises the six components of stress for each 3D element to a predefined value. With an incomplete set of measured input values, it is unlikely that force and moment balance will be satisfied. As a result, the Finite Element software generates a balanced solution which deviates from the measured values. Since it is not possible to measure a complete residual stress distribution, an iterative process was used instead. The initial residual stress distribution entered into the model was adjusted until the relative error between the measured values and the Abaqus solution at specified control points, defined at different locations within the laser peened area and through the thickness, was smaller than 1%. This allowed to achieve the desired residual stress distribution not just over the model surface, but also on each layer of elements through the thickness. A uniform in-depth residual stress profile was chosen for this study, which according to the residual stress results presented in the next chapter provided a good approximation of the real residual stress distribution. Finally, only the σ_y and σ_x components of

the measured compressive residual stress were introduced into the model, leaving the software free to calculate the balancing tensile residual stresses. The residual stress target values were obtained by averaging the neutron diffraction and contour method measurements averaged through the thickness at Point 1 (Figure 2): $\sigma_y = -146$ MPa and $\sigma_x = -98$ MPa. Thickness-averaged residual stresses have been successfully applied in the literature when modelling fatigue crack growth, as reported in [25].

3.2 Crack Growth Modelling

After the residual stress was introduced, external load was applied with a pressure boundary condition at the top surface to simulate fatigue loading (Figure 6). For each crack length, both the maximum and minimum loading conditions (σ_{max} and σ_{min}) were applied to calculate the corresponding maximum and minimum cyclic stress intensity factors ($K_{max,TOT}$ and $K_{min,TOT}$), according to the Modified Virtual Crack Closure Technique [26]. The forces and displacements extracted from the FE software were then processed with MATLAB to generate fatigue crack growth and fatigue life predictions.
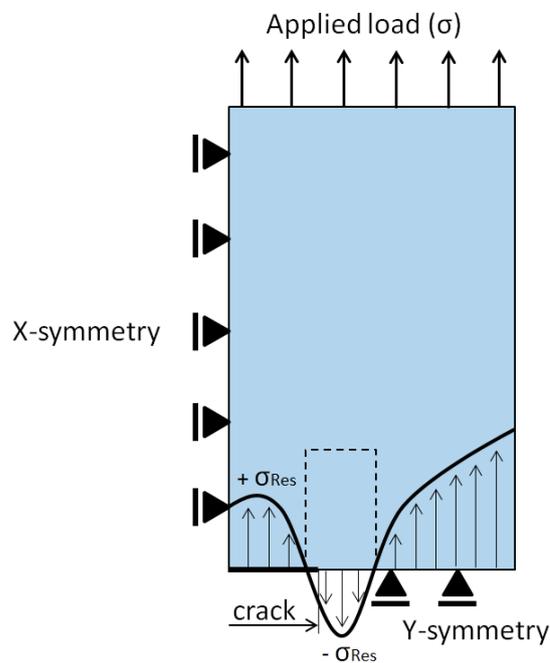

Figure 6 – Fatigue crack growth model boundary conditions

Crack propagation was simulated by progressively releasing the symmetry boundary condition applied on the nodes ahead of the crack tip. Using this scheme, the crack length was increased in 1 mm increments

from 4 mm – the initial crack length after precracking – to 70 mm. The final crack length was chosen averaging the crack length at failure on the fractured specimens. This approach was preferred to using a failure condition since all the measured crack lengths at failure were similar. The crack front shape was assumed to be straight and the crack was uniformly extended during propagation, in agreement with the work of many other researchers when modelling through-cracks [27,28].

3.3 Crack Growth Predictions

Three fatigue crack growth prediction methods were compared in this work: the Superposition method, the Modified Superposition method, and the Newman method.

<u>Superposition method</u>

The total stress intensity factor range and total stress ratio were calculated according to Eq. (3) and Eq. (4), respectively. An effective stress intensity factor range, which is a function of the total stress ratio, was then calculated according to the Walker equation [29]:

$$\Delta K_{eff} = \left[\frac{\Delta K_{TOT}}{(1-R_{TOT})^{1-\gamma}}\right] \qquad (8)$$

where γ is a fitting parameter that is experimentally determined [29].

<u>Modified superposition method</u>

The total stress intensity factor range and total stress ratio were calculated according to Eq. (5) and Eq. (6), respectively. The crack closure mechanism was simulated using a hard contact between the crack surface and a defined 3D rigid analytical shell lying on the Y symmetry pane and constrained to a reference point which was fixed with encastre boundary conditions. These constraints prevented crack surfaces from overlapping and therefore the generation of negative values for the stress intensity factor range. As in the Superposition method, the effective stress intensity factor range was calculated according to Eq. (8).

<u>Newman method</u>

The total stress intensity factor range and total stress ratio were calculated according to Eq. (3) and Eq. (4), respectively. The effective stress intensity factor range was then calculated according to the Newman analytical equations [16]:

$$\Delta K_{eff} = \left[\frac{(1-\sigma_{op}/\sigma_{max})}{1-R_{TOT}}\right]\Delta K_{TOT} \qquad (9)$$

$$\frac{\sigma_{op}}{\sigma_{max}} = A_0 + A_1 R_{TOT} + A_2 R_{TOT}{}^2 + A_3 R_{TOT}{}^3 \; for \; R_{TOT}{\geq}0 \qquad (10)$$

$$\frac{\sigma_{op}}{\sigma_{max}} = A_0 + A_1 R_{TOT} \; for \; R_{TOT}{<}0 \qquad (11)$$

where

$$A_0 = (0.825 - 0.34\alpha + 0.05\alpha^2)\left[\cos\left(\frac{\pi\sigma_{max}}{2\sigma_0}\right)\right]^{\frac{1}{\alpha}} \qquad (12)$$

$$A_1 = (0.415 - 0.071\alpha)\frac{\sigma_{max}}{\sigma_0} \qquad (13)$$

$$A_2 = 1 - A_0 - A_1 - A_3 \qquad (14)$$

$$A_3 = 2A_0 + A_1 - 1 \qquad (15)$$

and

$$\sigma_0 = \frac{\sigma_{YS}+\sigma_{UTS}}{2} \qquad (16)$$

For each method, the crack growth rate da/dN was determined from the calculated effective stress intensity factor range ΔK_{eff} using a table lookup approach as suggested in [17]. The coefficients, presented in Table 4 and

Table 5, were obtained from fatigue tests on several baseline (unpeened) specimens using different stress ratios (R=0.1, 0.3 and 0.6).

Table 4 – Walker's lookup table coefficients

ΔK_{eff} [MPa√m]	da/dN [m/cycle]
6.37	1.59×10^{-8}
13.65	3.72×10^{-7}
29.51	1.30×10^{-6}
63.81	3.47×10^{-5}

Table 5 – Newman's lookup table coefficients

ΔK_{eff} [MPa√m]	da/dN [m/cycle]
4.67	1.94×10^{-8}
9.78	3.71×10^{-7}
20.48	1.20×10^{-6}
42.87	2.43×10^{-5}

4 Results and Discussion

4.1 Residual Stress Results

The results obtained using neutron diffraction and the contour method for the σ_y component of residual stress at Points 1, 2, 3 (depth profiles) and along Line 1 (through thickness averages), are presented in Figure 7 and Figure 8, respectively.
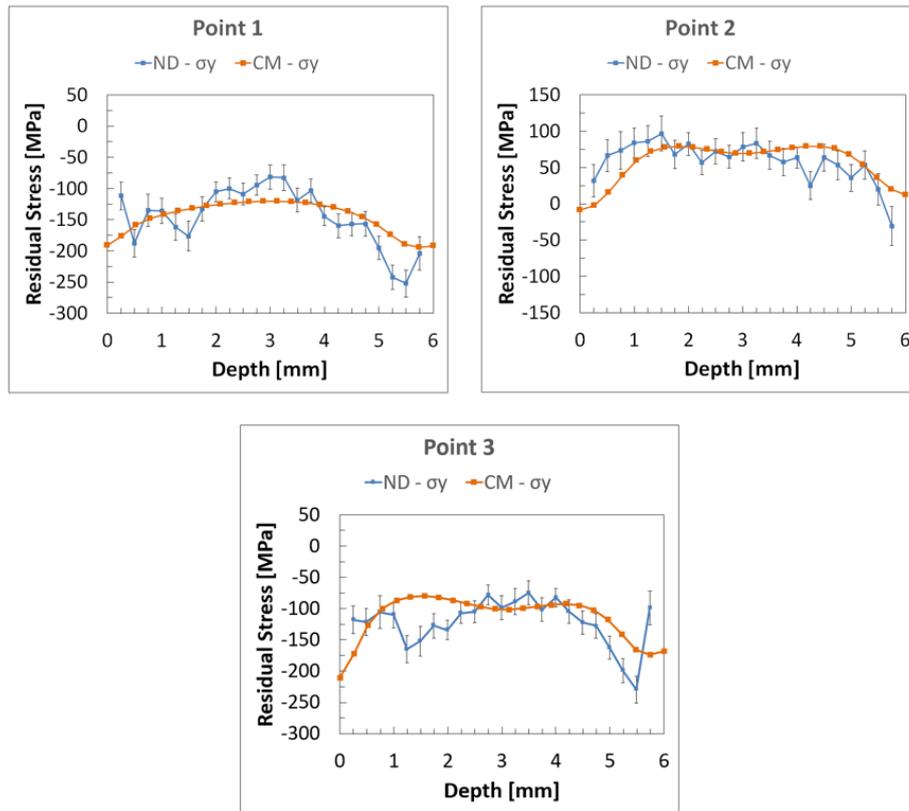
Figure 7 – Comparison between Neutron Diffraction (ND) and Contour Method (CM) residual stress results: σ_y at Points 1, 2 and 3 (Figure 2)
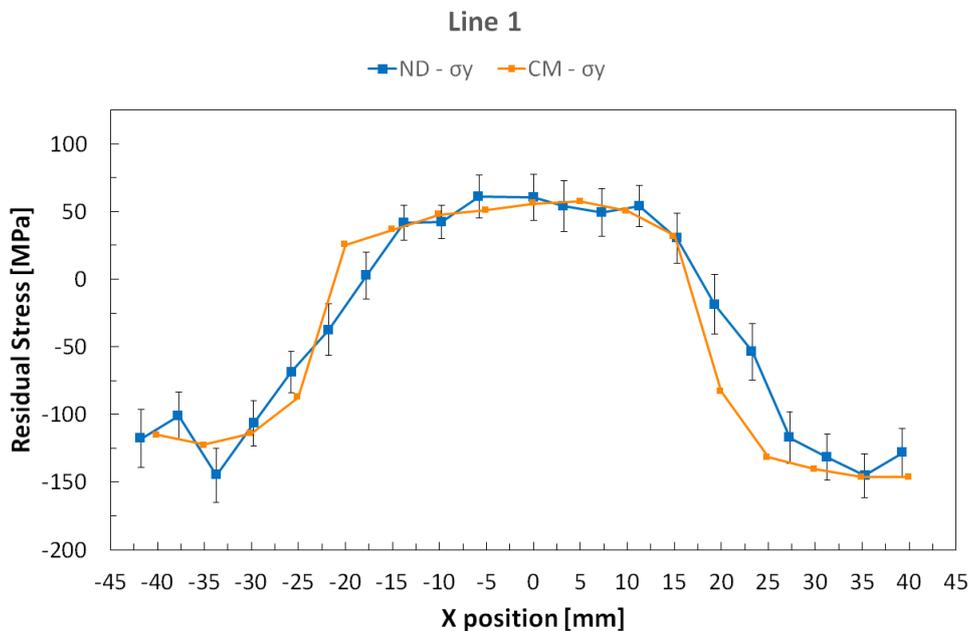

Figure 8 – Comparison between Neutron Diffraction (ND) and Contour Method (CM) residual stress results: σ_y averaged through the thickness along Line 1 (Figure 2)

The two methods are in generally good agreement. The through-thickness residual stress distributions at Points 1 and 3 (Figure 7) show a fully compressive residual stress profile resulting from the laser peening process. Its variation with depth furthermore, highlights a fairly constant residual stress profile which is matching the through-thickness averaged values, with the exception of the near-surface areas where a higher gradient can be noticed.

The through-thickness averaged residual stress distribution along Line 1 (Figure 8**Error! Reference source not found.**) exhibits compression within the laser shock peened areas with values up to −146 MPa, balanced by tension (up to 60 MPa) near the centre of the specimen between the laser shock peening patches (–25 mm < X < 25 mm). A small discrepancy between the two techniques in Figure 8 is visible in the transition zone (15 mm < X < 25 mm) where the neutron diffraction measurements show a somewhat lower level of compression, possibly because of microstructural changes which can lead to changes in the lattice parameter which are not due to residual stress.

A comparison between the initial FE residual stress solution (un-cracked body), the neutron diffraction results, and the contour method results is presented in Figure 9**Error! Reference source not found.** for the Y component of residual stress (σ_y) averaged through the thickness along Line 1.
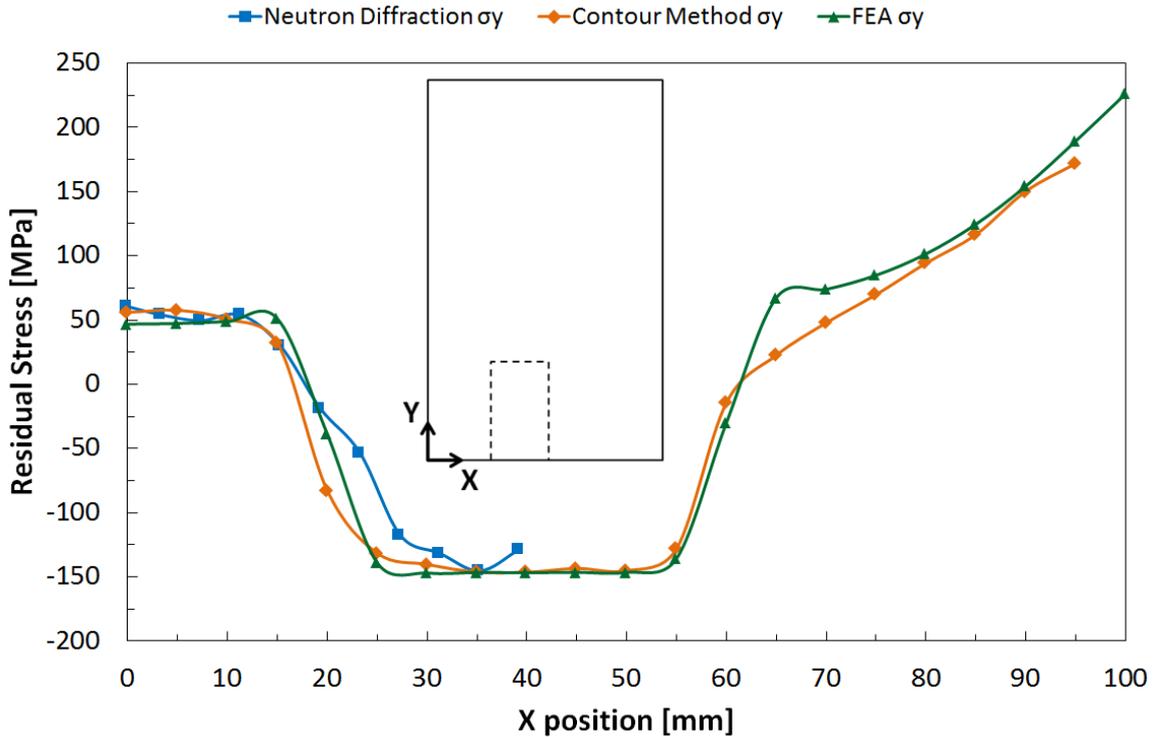
Figure 9 – Comparison between initial Finite Element residual stress (un-cracked body), and the neutron diffraction and contour method results for σ$_y$, averaged through the thickness

Figure 9**Error! Reference source not found.** shows very good agreement between the FE solution and the experimental measurements, not only in terms of the compressive residual stress inside the laser peened area, but also in terms of the balancing tensile residual stress in the rest of the section.

4.2 Fatigue Crack Growth Test Results

Two samples were tested for each of the unpeened and laser peened conditions with the same loading, showing little scatter in the fatigue results. This allowed to increase the confidence in the crack growth data collected, despite the small amount of specimens available. The fatigue life of the treated components was found to be about 4× that of the pristine unpeened material, as shown in Figure 10.
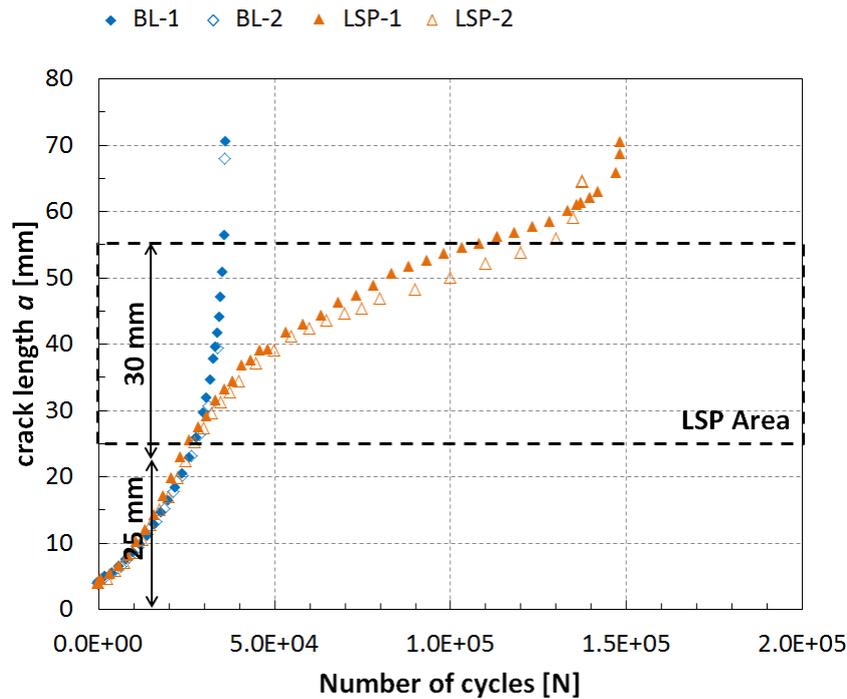
Figure 10 – Fatigue crack growth rate results, *a vs N* for the baseline (BL) and laser-peened (LSP) specimens. The peened area spanned a distance from the centre of the sample equivalent to crack lengths between 25 and 55 mm.

The figure also shows that crack propagation in the laser peened samples (LSP-1 and LSP-2) was slightly faster than in the untreated components (BL-1 and BL-2) in the region between the laser peened areas, due to the balancing tensile residual stress from the peening treatment. This effect is more clearly revealed in the zoomed view in Figure 11, where only the early part of crack propagation (up to a crack length *a* of 40 mm) is shown. Once the crack entered the peened region, the decrease in crack growth rate more than compensated for the crack acceleration in the unpeened area, resulting in the four-fold increase in fatigue life.

The crack growth rate is plotted as a function of ΔK in Figure 12. The data show that the crack growth rate is significantly lower in the LSP specimens that in the unpeened baseline specimens when the crack tip is inside the laser shock peened area owing to the compressive residual stress acting along the crack opening direction (σ_y) in this region. The crack growth rate was lowest at the end of the treated area (*a* =

55 mm), where da/dN was 13% of its value just before the crack entered the compressive section of the residual stress field due to peening.
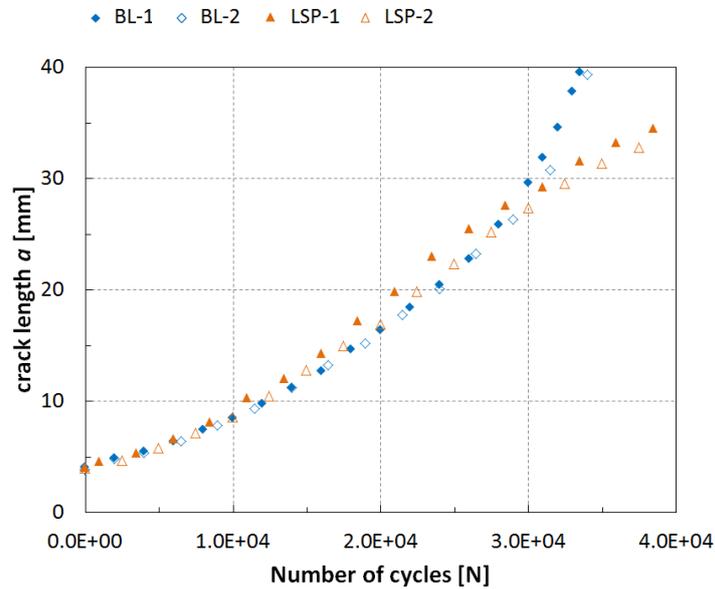

Figure 11 – Fatigue crack growth acceleration due to tensile residual stress. The laser peened (LSP) samples show faster growth than the baseline (BL) samples before the crack intersects the laser peened region at a crack length of ~25 mm
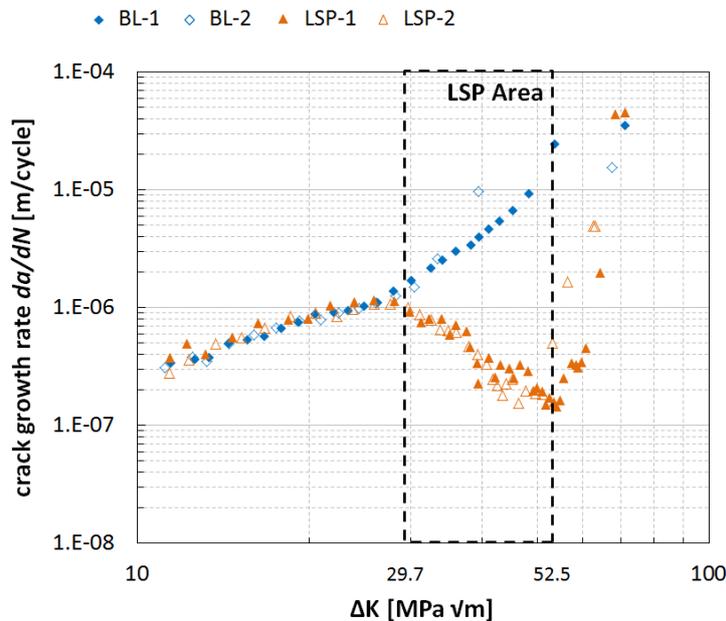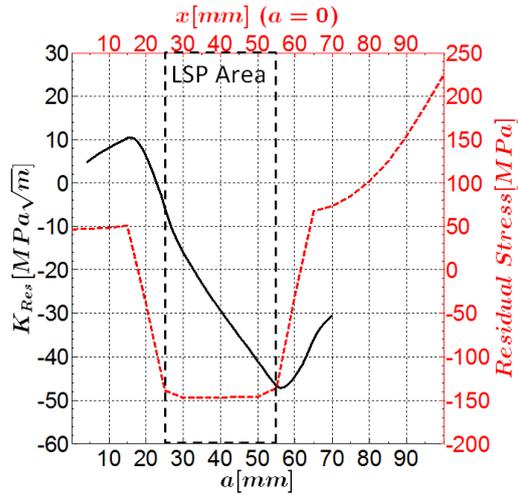

Figure 12 – Fatigue crack growth rate, da/dN *vs* ΔK. The crack growth rate decreases significantly in the laser peened samples (LSP) once the crack enters the peened area. The baseline (BL) samples show steady acceleration of the crack as it grows.
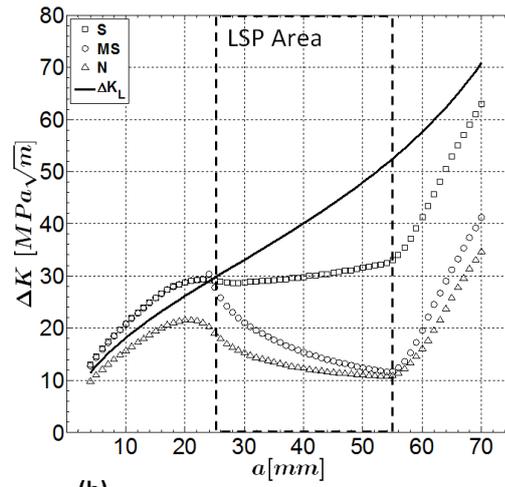
4.3   Fatigue Crack Growth Predictions

The crack growth rates predicted using the three modelling approaches are presented in Figure 13, which is divided into 7 sub-figures showing K_{Res} vs x and the *Residual Stress* vs a in (a); ΔK vs a in (b); the *Stress Intensity Factor* vs a in (c); the *Stress Ratio* vs a in (d); da/dN vs a in (e); da/dN vs ΔK in (f) and σ_{op}/σ_{max} vs a according to Eq. (10) and Eq. (11) in (g).
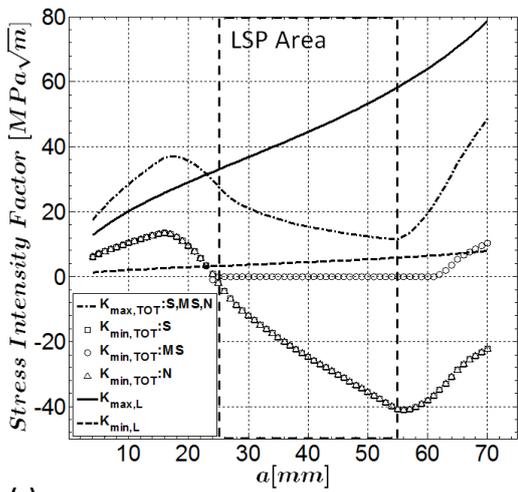
The residual stress intensity factor K_{Res} highlighted in Figure 13(a) (black solid line) follows the main trend shown by the initial residual stress distribution, but with a smoother profile. Figure 13(b) shows the variation of effective stress intensity factor range ΔK_{eff} with crack length obtained using the three modelling approaches, together with the nominal ΔK from the loading conditions, ΔK_L. The reduction in ΔK due to the compressive residual stress in the peened area is greatest using the Modified Superposition method, slightly less pronounced using the Newman approach, and much weaker for the Superposition approach. Figure 13(c) shows how the stress intensity factor varies with crack length for the three approaches. The three approaches show identical values for $K_{max,TOT}$, with no crack closure occurring at the maximum applied load. In contrast, while the Superposition and Newman approaches predict identical values for $K_{min,TOT}$ which becomes strongly negative in the peened region, $K_{min,TOT}$ cannot become negative in the Modified Superposition approach as this approach imposes rigid crack closure. Similar behaviour can be observed in Figure 13(d): the total stress ratio for all three approaches is identical up to the start of the peened region, at which point it becomes negative for the Superposition and Newman approaches, but is constrained to be zero for the Modified Superposition approach. Though the nominal applied stress ratio was 0.1, the tensile residual stress acting between the specimen centre and the laser peened area pushes the predicted value up to 0.36 in this region.
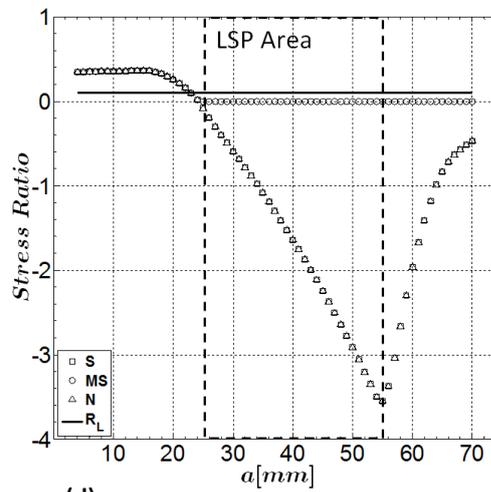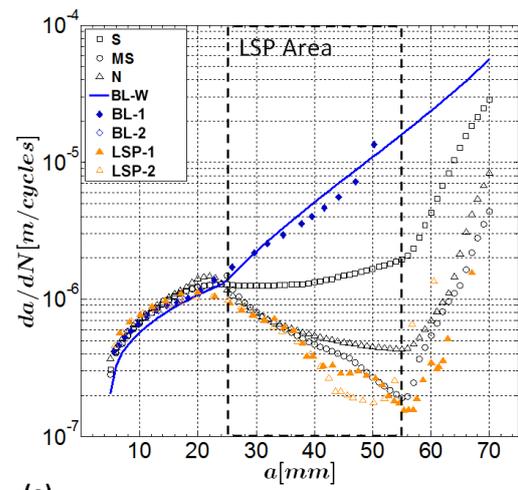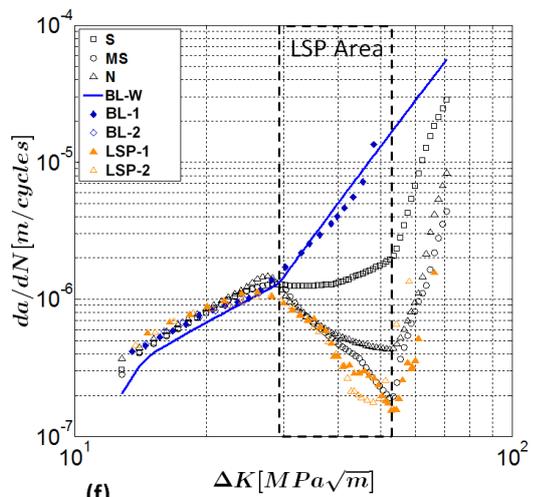
(a)

(b)

(c)

(d)

(e)

(f)

(g)

Figure 13 – (a) K_{Res} vs *x* and *Residual Stress* vs *a*; (b) predicted ΔK vs *a* as a result of the applied

ΔK_L; (c) predicted *Stress Intensity Factor* vs *a*, (d) Predicted *Stress Ratio* vs *a*; (e) d*a*/d*N* vs *a* for

the experimental samples, along with the predicted crack growth rates from the three models

used; (f) d*a*/d*N* vs ΔK for the experimental samples, along with the predicted crack growth rates

from the three models used; (g) Predicted σ_{op}/σ_{max} vs *a* from Eq. (10) and Eq. (11);

S=Superposition method, MS=Modified Superposition method, N=Newman method, BL-W=

Predicted baseline with Walker equation

Figure 13(e) and (f) present the predicted crack growth rates together with the experimental data. The

baseline test results for BL-1 and BL-2 are also included, showing good agreement with predictions (BL-

W) apart from a small underestimation of the growth rate in the very early stages of crack propagation.

The Modified Superposition method (circular empty markers on the figure) gives the best predictions,

with most of the predicted values falling within a factor of 1.25 of the measured values. The maximum

deviation (within a factor of 2) occurs towards the end of the crack propagation, and therefore

corresponds to very long cracks approaching the critical length. Under these conditions, the model

assumptions may not be valid, since region III of crack propagation is approached. Since these later

stages of crack propagation account for a small portion of the fatigue life, the large discrepancy between

experimental results and model predictions do not significantly affect the fatigue life prediction.

The crack growth rates predicted using the Newman and Modified Superposition methods are very similar up to a crack length of ~35 mm. Beyond this value, the Newman method predicts higher growth rates, eventually converging again with the Modified Superposition results for crack lengths greater than ~60 mm. The Superposition method heavily overestimates the growth rate within the laser shock peened area, giving the worst results. Figure 13(g) presents the normalised crack opening stresses σ_{op}/σ_{max} as a function of the crack length a, calculated with the Newman method. Results follow the total stress ratio trend shown in Figure 13(d), since this is the only parameter affected by the residual stress in Eq. (10) and Eq. (11). The a vs N curves presented in Figure 14 show that the Modified Superposition method provides the most accurate fatigue life estimation with a prediction of 128520 cycles, 7% more conservative than LSP-2 (137565 cycles). Results from the Newman model are even more conservative, with a predicted life of 94246 cycles, 31% less than the experimental value. The Superposition method shows almost no improvement in fatigue life from the laser peening process, with a predicted life of 50997 cycles, only slightly higher than the baseline results.
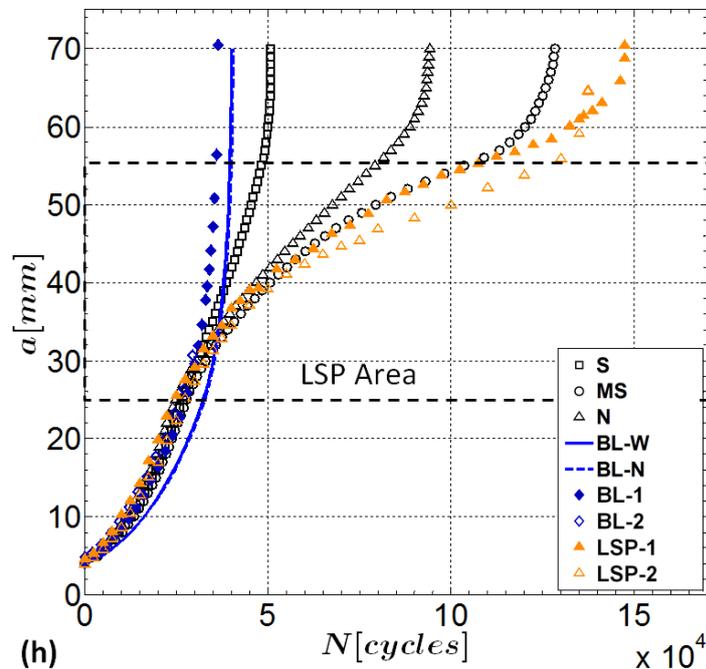

(h)

Figure 14 – *a* **vs** *N***; S=Superposition method, MS=Modified Superposition method, N=Newman method, BL-W= Predicted baseline with Walker equation, BL-N= Predicted baseline with Newman equation**

Conclusions

The effect of laser shock peening on fatigue crack growth in an aerospace aluminium alloy was studied by placing two laser-peened patches onto a middle-crack tension specimen made of AA2524-T351, with a thickness of 6 mm. The benefits introduced by the laser peening treatment in terms of fatigue performance, fatigue life, and crack growth were studied with both experimental testing and numerical modelling. The residual stress resulting from the laser peening process was determined using neutron diffraction and the contour method. This information was incorporated into a linear-elastic fracture mechanics finite element model to accurately simulate fatigue crack growth in the presence of the residual stress field. Several fatigue crack growth prediction models were used, namely the Superposition, the Modified Superposition, and the Newman methods. The following conclusions can be drawn:

1. The Residual stress measured along the crack opening direction, σ_y, was compressive through the thickness inside the laser peened areas, with through-thickness averaged values up to -146 MPa. The compression introduced by the laser peening treatment was balanced by a tensile residual stress field between the laser peened patches, with through-thickness averaged values up to 60 MPa.

2. The laser peened samples had fatigue lives about 4x those of unpeened specimens. The compressive residual stress introduced by the laser peening treatment caused a dramatic decrease in fatigue crack growth rate when the crack tip entered the peened region, so extending the overall fatigue life. A small fatigue crack growth rate increase was observed at the beginning of crack propagation, when the crack propagated within the tensile residual stress field that balances the compressive stress in the peened region.

3. Fatigue crack growth predictions showed very good agreement with experimental data as long as a crack closure mechanism was considered, such as in the Modified Superposition and Newman methods. The former, which was realised in the FE model by preventing crack surfaces from overlapping, provided the best results, predicting a fatigue life only 7% shorter than observed experimentally. The latter, based

on the plasticity-induced crack closure mechanism, generated slightly more conservative estimates of fatigue life.

In summary, we have demonstrated that laser peening can be used successfully to extend the fatigue life of aerospace aluminium in a section thickness relevant to wing cover applications, leading potentially to reduced maintenance costs or to weight savings. If the residual stress distribution from the laser peening has been fully characterized by experiment furthermore, a relatively simple FE model can provide a suitably accurate and conservative prediction of the fatigue life.

Acknowledgments

References

[1]   Montross CS, Wei T, Ye L, Clark G, Mai YW. Laser shock processing and its effects on microstructure and properties of metal alloys: A review. Int J Fatigue 2002;24:1021–36. doi:10.1016/S0142-1123(02)00022-1.

[2]   Fitzpatrick ME, Lodini A. Analysis of Residual Stress by Diffraction using Neutron and Synchrotron Radiation. 2003.

[3]   Macherauch E, Kloss KH. Proceedings of the International Conference on residual Stresses. Garmisch-Partenkirchen, FRG 1986:167–74.

[4]   Withers PJ, Bhadeshia HKDH. Residual stress. Part 1–measurement techniques. Mater Sci Technol 2001;17:355–65. doi:10.1179/026708301101509980.

[5]   Reimers W, Pyzalla AR, Schreyer A, Clemens H. Neutrons and Synchrotron Radiation in Engineering Materials Science. WILEY-VCH Verlag GmbH & Co. KGaA, Weinheim; 2008.

[6]   Achintha M, Nowell D. Eigenstrain modelling of residual stresses generated by laser shock peening. J Mater Process Technol 2011;211:1091–101. doi:10.1016/j.jmatprotec.2011.01.011.

[7]   LaRue JE, Daniewicz SR. Predicting the effect of residual stress on fatigue crack growth. Int J Fatigue 2007;29:508–15. doi:10.1016/j.ijfatigue.2006.05.008.

[8]   Bueckner HF. The Propagation of Cracks and the Energy of Elastic Deformation. Trans Am Soc Mech Eng 1958;80:1225--1230.

[9]   Underwood JH, Pook LP, Sharples JK. Fatigue-Crack Propagation Through a Measured Residual Stress Field in Alloy Steel. Flaw Growth Fract 1977;ASTM STP 6:402–15.

[10]   Fukuda S, Yasuyuki T. An Experimental Study of Redistribution of Welding Residual Stress with Fattgue Crack Extension 1978:67–72.

[11]   Chandawanich N, Sharpe WN. An experimental study of fatigue crack initiation and growth from coldworked holes. Eng Fract Mech 1979;11:609–20. doi:http://dx.doi.org/10.1016/0013-7944(79)90122-X.

[12]   Lam YC, Lian KS. The effect of residual stress and its redistribution of fatigue crack growth. Theor Appl Fract Mech 1989;12:59–66. doi:http://dx.doi.org/10.1016/0167-8442(89)90015-3.

[13]   Parker AP. Stress Intensity Factors, Crack Profiles, and Fatigue Crack Growth Rates in Residual Stress Fields. Residual Stress Eff Fatigue 1982;STP 776:13–31. doi:10.1520/STP30095S.

[14]   Wolf E. Fatigue crack closure under cyclic tension. Eng Fract Mech 1970;2:37–45. doi:http://dx.doi.org/10.1016/0013-7944(70)90028-7.

[15]   Newman JC. A crack-closure model for predicting fatigue crack growth under aircraft spectrum loading. Methods Model Predict Fatigue Crack Growth under Random Load 1981;748:53–84.

doi:10.1520/STP28334S.

[16]   Newman JC. A crack opening stress equation for fatigue crack growth. Int J Fract 1984;24. doi:10.1007/BF00020751.

[17]   Hill MR, Kim J. Fatigue Crack Closure in Residual Stress Bearing Materials. J ASTM Int 2012;9:65–86. doi:10.1520/JAI104071.

[18]   Garcia C, Lotz T, Martinez M, Artemev A, Alderliesten R, Benedictus R. Fatigue crack growth in residual stress fields. Int J Fatigue 2016;87:326–38. doi:10.1016/j.ijfatigue.2016.02.020.

[19]   Kashaev N, Ventzke V, Horstmann M, Chupakhin S, Riekehr S, Falck R, et al. Effects of laser shock peening on the microstructure and fatigue crack propagation behaviour of thin AA2024 specimens. Int J Fatigue 2017;98:223–33. doi:10.1016/j.ijfatigue.2017.01.042.

[20]   SAE International. AMS4296B 2012.

[21]   Prime MB, Gonzales AR. the Contour Method: Simple 2-D Mapping of Residual Stresses. Sixth Int Conf Residual Stress Int Conf Residual Stress July 10-12, 2000;836:617–24.

[22]   ASTM Standard E647 − 13a. Standard Test Method for Measurement of Fatigue Crack Growth Rates. Am Soc Test Mater 2014:1–50. doi:10.1520/E0647-13A.2.

[23]   Dasssult Systemes. ABAQUS User's Manual, version 6.14 2014.

[24]   MathWorks. MATLAB User's Manual, version R2013b 2013.

[25]   Liljedahl CDM, Zanellato O, Fitzpatrick ME, Lin J, Edwards L. The effect of weld residual stresses and their re-distribution with crack growth during fatigue under constant amplitude loading. Int J Fatigue 2010;32:735–43. doi:10.1016/j.ijfatigue.2009.10.012.

[26]   Krueger R, Krueger R. The Virtual Crack Closure Technique : History , Approach and Applications. Hampton: 2002.

[27]   Solanki K, Daniewicz SR, Newman JC. Finite element analysis of plasticity-induced fatigue

crack closure: an overview. Eng Fract Mech 2004;71:149–71. doi:10.1016/S0013-7944(03)00099-7.

[28]   Gozin MH, Aghaie-Khafri M. 2D and 3D finite element analysis of crack growth under compressive residual stress field. Int J Solids Struct 2012;49:3316–22. doi:10.1016/j.ijsolstr.2012.07.014.

[29]   Walker EK. The effect of stress ratio during crack propagation and fatigue for 2024-T3 and 7075-T6 aluminum. ASTM STP, Am Soc Test Mater 1970:1–14. doi:10.1520/stp32032s.